DOI https: //doi. org/10.1007/s11595-021-2399-5

Aqueous Preparation of Highly Dispersed Hydroxyapatite Nanorods for Colloidal Liquid Crystals

XIONG Yan[1], TAN Peng[1], LIU Qi[2], LIU Kaixuan[3], TAN Junjun[1*]

(1. Hubei Provincial Key Laboratory of Green Materials for Light Industry, Hubei University of Technology, Wuhan 40068, China; 2. Jiangxi Provincial Engineering Research Center for Multifunction Zirconia Materials, Jiangxi Size Materials Co., Ltd, Jiujiang 332500, China; 3. Jiangxi De Corematrix Co., Ltd., Jiujiang 332500, China)

Abstract: Hydroxyapatite (HA) nanorods were synthesized using a citrate-assisted hydrothermal method. NaH_2PO_4, Na_2HPO_4, and Na_3PO_4 were used as the phosphate sources and the influences of pH value were investigated. The XRD results show that pure hexagonal HA can be synthesized using $Na_3PO_4{\cdot}12H_2O$ as the phosphate source with the citrate solution pH ranging from 5.0 to 7.6. The zeta potential evaluation demonstrates that as-synthesized HA nanorods are colloidally stable and the aqueous dispersion can be maintained homogenous without any sediment or creaming for more than at least a month. The Ca/P molar ratio of the HA nanorods is about 1.60, indicating that the HA nanorods are calcium-deficient hydroxyapatite. Besides, owing to the excellent colloidal stability and rod-like morphology with a high aspect ratio (>6), the HA aqueous dispersion undergoes a phase transition from an isotropic state to a liquid crystalline state upon increasing the particle concentration to 17wt%. The completely liquid crystalline phase forms when the particle concentration reaches above 30wt%.

Key words: hydroxyapatite; liquid crystal; colloidal stability

1 Introduction

Hydroxyapatite (HA, $Ca_{10}(PO_4)_6(OH)_2$) is the most stable calcium phosphate phase under physiological conditions and is the model compound used to denote the mineral components of bone and dentin because of its excellent biocompatibility and biological activity and strong ion exchange capacity[1,2]. Owing to these merits, HA is widely used in a range of fields, such as bone tissue engineering[3,4], heavy metal ion absorption[5,6], fluorescent materials[7,8], protein separation[9,10] and drug carriers[11-13]. Among these bio-related applications, the morphology, size, crystallinity, or aqueous colloidal stability of HA nanoparticles often must be controlled to meet specific requirements. Highly crystalline, monodisperse HA nanorods with excellent aqueous colloidal stability and high aspect ratio have been constantly pursued as desirable basic units. However, considering the aforementioned multiple requirements and the biocompatibility of additives in the synthesis process, there are not many options available to achieve these materials.

Recently, the effect of sodium citrate on the growth of hydroxyapatite nanocrystals has received increasing attention. This increase in attention is partly due to the discovery of an abundance of citrate molecules strongly bound to natural bone apatite surface, as determined by solid-state NMR analysis, indicating that citrate molecules play a significant role in the formation of HA nanocrystals and the well-dispersed state of HA in bone tissue[14]. Another reason for this increased attention is that numerous studies have shown that citrate molecules can strongly control the morphology and size of HA nanocrystals during artificial synthesis[15-17]. Moreover, citrate molecules are a natural organic acid with excellent biocompatibility, serving as a very safe and abundant resource for bio-related applications[18].

Using a citrate-assisted hydrothermal method, bio-inspired citrate-carbonate-apatite nanocrystals have been prepared by batch thermal de-complexing of calcium/citrate/phosphate/carbonate solutions[19]. The authors of this study found that the resultant nanocrys-

(Received: Apr. 11, 2020; Accepted: Aug. 20, 2020)

XIONG Yan(熊焰): Prof.; E-mail: xiongyan1980@hotmail.com

*Corresponding author: TAN Junjun(谭军军): Assoc. Prof.; E-mail: tanjunjun2011@hbut.edu.cn

Funded by the National Natural Science Foundation of China (Nos. 21203059 & 51402097), the Natural Science Foundation of Hubei Province (No. 2018CFB710), the National Training Program of Innovation and Entrepreneurship for Undergraduates (201710500010), and the Opening Fund (No. 201907B12) of Hubei Provincial Key Laboratory of Green Materials for Light Industry, Hubei University of Technology

tals were composed of a well-ordered carbonate-substituted apatite core embedded in a non-apatite hydrated layer containing citrate ions. This layer progressively transformed into a more stable apatite domain upon maturation. Meanwhile, with the aid of citrate, before hydrothermal treatment, the mixture was a homogeneous metastable solution, avoiding the instantaneous nucleation of calcium phosphate[20]. On the other hand, an increase in temperature resulted in a gradual and homogeneous release of calcium ions leading to the formation of amorphous calcium phosphate that transforms into crystalline apatite platelets with citrate adsorbed on the surface[16,21].

Considerable effort has been put forth to investigate the various factors that affect the formation of HA in the citrate-assisted hydrothermal method. These factors include the molar ratio of calcium to citrate[22,23], hydrothermal temperature and time[24], the synergistic effect of citrate with other compounds[17,25,26], and ion doping[27-29]. In addition to the above experimental factors, the pH of citrate solution and the type of phosphate are also important for the solution-based synthesis of HA nanoparticles, which affects the formation of precursors, conversion of precursors to hydroxyapatite, phase purity of the crystal phase, particle size, the morphology of the final product, *etc*[30-32]. Previous studies have often emphasized the role of citrate ions in the citrate-assisted hydrothermal synthesis, which involves complexation with calcium ions, surface modification and inhibition of the crystallization of sodium citrate. Nearly all previous studies have been based on pure sodium citrate or pure citric acid. By controlling the pH of the citrate solution and the type of phosphate, a relatively stable pH environment should be achieved, which would be helpful for the synthesis of highly dispersed and uniform HA nanorods. Unfortunately, thus far, there has been a lack of systematic studies to reveal the effect on the growth of HA in the citrate-assisted hydrothermal synthesis.

In the present work, the influence of pH of the citrate solution and the type of phosphate on the phase structure, morphology, and colloidal stability of the resultant compounds has been systematically studied. The experimental conditions at which highly crystalline, colloidally stable, and high aspect ratio HA nanorods could be obtained were determined. In addition, the possible liquid crystal phase transition of HA nanorods colloidal dispersion was preliminarily investigated.

2 Experimental

2.1 Raw materials

Calcium nitrate tetrahydrate ($Ca(NO_3)_2•4H_2O$, ≥99.0%), sodium phosphate monobasic dihydrate ($NaH_2PO_4•2H_2O$, ≥99.0%), sodium phosphate dibasic dodecahydrate ($Na_2HPO_4•12H_2O$, ≥99.0%), sodium phosphate tribasic dodecahydrate ($Na_3PO_4•12H_2O$, ≥98.0%), sodium citrate tribasic dihydrate ($C_6H_5Na_3O_7•2H_2O$, ≥99.0%), citric acid monohydrate ($C_6H_8O_7•H_2O$, ≥99.5%), absolute ethanol (C_2H_6O, ≥99.7%) and sodium hydroxide (NaOH, ≥97.0%) were purchased from Aladdin Reagent Co., Ltd. Shanghai, China. All chemicals were used as received without further purification. Deionized water was used throughout the study.

2.2 Preparation of colloidal HA nanorod dispersions

HA nanorods were prepared using a citrate-assisted hydrothermal method. In a typical experiment, a citrate solution with a fixed pH value (0.01 mol, 10 g H_2O) was slowly added to an aqueous solution of $Ca(NO_3)_2•_4H_2O$ (0.008 mol, 10 g H_2O) with continuous stirring over 10 min. Then, an aqueous solution of phosphate (0.0048 mol, 10 g H_2O) was slowly added to the mixture with vigorous stirring over 10 min. After that, the as-obtained mixed solution was transferred to a Teflon-lined stainless-steel autoclave with a 50 mL capacity. The solution in the autoclave underwent hydrothermal treatment at 180 ℃ for 6 h. After hydrothermal treatment, the autoclave was allowed to naturally cool down, and the resulting product was purified using a three-cycle centrifugation-washing process with deionized water and ethanol. Finally, part of the purified product was re-dispersed in deionized water to form an aqueous dispersion. The pH of the dispersion was adjusted to pH 9.5 by the addition of 0.1 M NaOH. The remainder of the sample was dried at 80 ℃ for 12 h to obtain a powder for future characterization.

Table 1 Detailed experimental parameters in present study

Sample code	HA11	HA12	HA13	HA14	HA21	HA22	HA23	HA24	HA31	HA32	HA33	HA34
pH value	5.0	5.5	6.0	7.6	5.0	5.5	6.0	7.6	5.0	5.5	6.0	7.6
Calcium source	$Ca(NO_3)_2•4H_2O$											
Phosphate source	$NaH_2PO_4•2H_2O$					$Na_2HPO_4•2H_2O$				$Na_3PO_4•12H_2O$		

For the sake of simplicity, HA nanoparticles synthesized under various experimental conditions will henceforth be labeled HA*xy*, where *x* is the type of phosphate and *y* is the code of the pH of the citrate solution. For example, HA11 refers to a sample synthesized using a citrate buffer solution with a pH of 5.0 and NaH_2PO_4 as the phosphate source. The detailed experimental parameters are listed in Table 1.

2.3 Preparation of colloidal HA liquid crystals

The HA colloidal dispersion was concentrated with a rotary evaporator and then diluted into a series of samples with different particle concentrations. These dispersions were analyzed as follows: 1 mL sample of a typical dispersion was taken using a pipette, and then, the pipette tip was dried in a vacuum oven at 80 ℃ for 24 h. The particle concentrations of the HA nanorods in the dispersions were calculated using the differences between the weights of the original pipette tips and those of the tips that were dried after adding the dispersion.

2.4 Characterization

Phase identification of the samples was examined by X-ray diffraction (XRD, Empyrean, PANalytical B.V., Almelo, Netherlands) with CuKα radiation. The microstructures were characterized by scanning electron microscopy (FE-SEM, SU8010, Hitachi High-Technologies Co., Japan) and high-resolution transmittance electron microscopy (HRTEM, Tecnai G2/F20, FEI Co., USA). The length (L) and diameter (D) of the HA nanorods were measured using a statistical method from three TEM images (at least 300 counts). The aspect ratio ($R_{L/D}$) of each nanorod is defined by the following equations:

$$<L>=\frac{\Sigma_1^n}{L} \tag{1}$$

$$<D>=\frac{\Sigma_1^n D}{n} \tag{2}$$

$$<R_{L/D}>=\frac{\Sigma_1^n L/D}{n} \tag{3}$$

$$\sigma_L=\frac{\sqrt{\frac{1}{n}\Sigma_1^n (L-<L>)^2}}{R_{L/D}} \tag{4}$$

$$\sigma_D=\frac{\sqrt{\frac{1}{n}\Sigma_1^n (D-<D>)^2}}{R_{L/D}} \tag{5}$$

$$\sigma_R=\frac{\sqrt{\frac{1}{n}\Sigma_1^n (R_{L/D}-<R_{L/D}>)^2}}{R_{L/D}} \tag{6}$$

where, $<L>$, $<D>$, and $<R_{L/D}>$ are the mean length, diameter, and aspect ratio of the HA nanorods, respectively. The values σ_L, σ_D, and s_R are the polydispersity of the length, diameter, and aspect ratio of the HA nanorods, respectively.

The colloidal stability of samples was evaluated by zeta potential measurement (nano-ZS90 zetasizer, Malvern Instruments Ltd., Malvern, UK). For the zeta potential measurements, the particle dispersion and pH of the sample dispersion are 0.5wt% and 9.5, respectively. No additional electrolytes were added to the samples for zeta potential measurements. The appearances of the 1wt% samples dispersed in the aqueous phase were recorded by taking photographs with a camera (Nikon, D7100). The macroscopic birefringence of HA dispersions with different particle concentrations was studied between crossed polarizers in cuvettes with a width of 2 mm that were filled with approximately 0.4 cm^3 of dispersion. The dispersion in the cuvette was sealed with liquid paraffin to prevent evaporation. The elemental contents of Ca and P in the samples were determined by inductively coupled plasma optical emission spectrometry (ICP-OES, Agilent 725, Agilent Technologies Co. Ltd., USA).

3 Results and discussion

3.1 Phase identification from XRD patterns

The XRD patterns of the resultants obtained from different citrate solution pH values and phosphate sources are shown in Fig.1. As shown in Fig.1(a), the detected diffraction peaks of the sample are indexed as a mixture of hexagonal HA (JCPDS# 86-0740) and an impurity phase when the phosphate source is NaH_2PO_4 and the pH of the citrate buffer solution ranges from 6.0 to 7. A further decrease in the pH of the citrate solution from 6.0 to 5.0 leads to a gradual diminishment of the typical diffraction peaks for HA. The pure HA phase was observed when the phosphate source is Na_2HPO_4 and the citrate solution pH value is 7.6, seen in Fig.1(b). However, the product purity is sensitive to the pH of the citrate solution. Upon further decreasing the pH of the citrate buffer solution from 6.0 to 5.0, the diffraction peaks of hexagonal HA gradually diminish. By comparisons, all the diffraction peaks of the final product are consistent with standard HA within

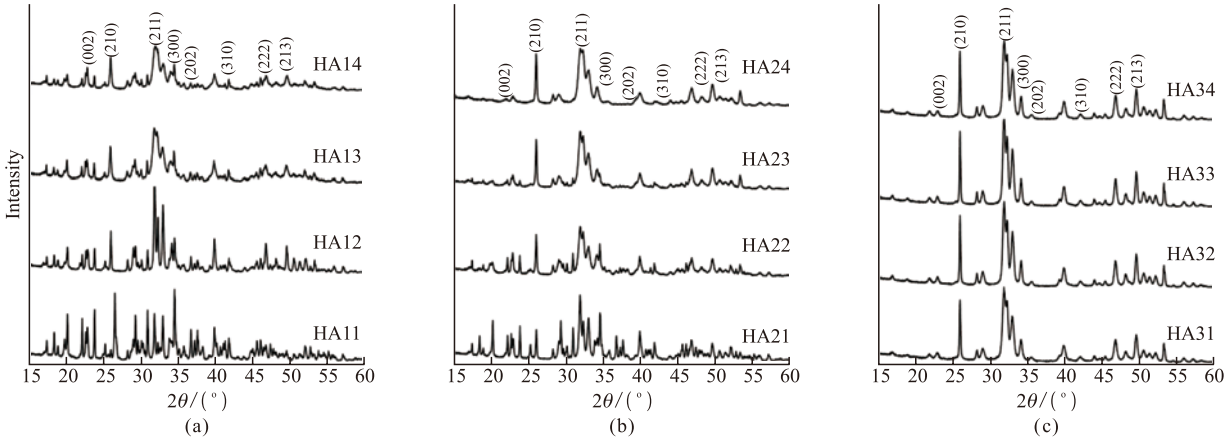

Fig.1 XRD patterns of the synthesized samples using (a) NaH_2PO_4, (b) Na_2HPO_4, and (c) Na_3PO_4 as the phosphate sources with pH values ranging 5.0-7.6

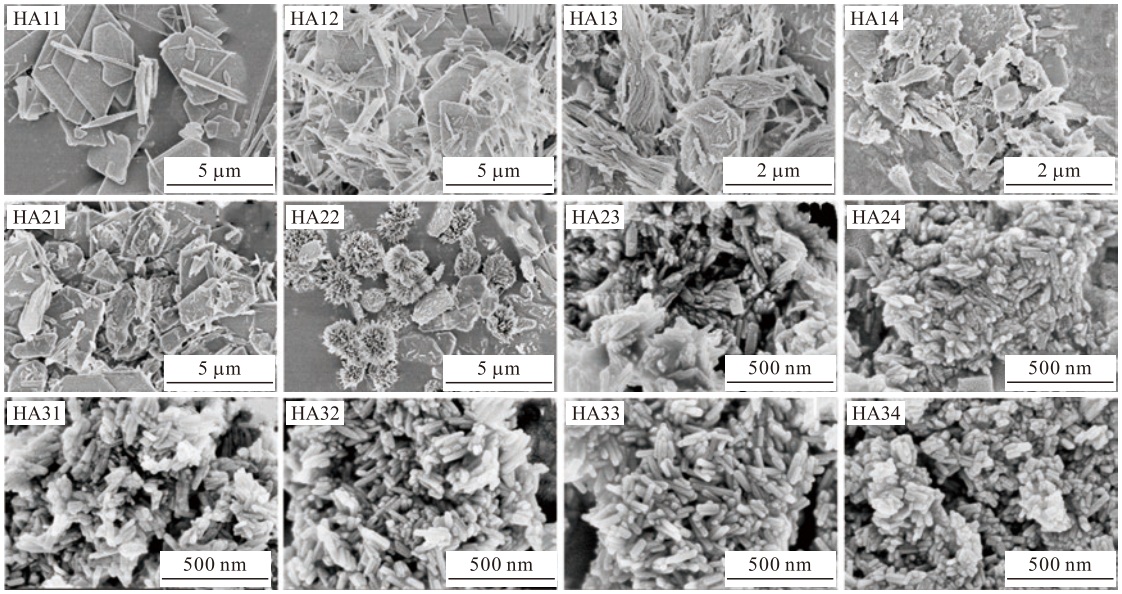

Fig.2 FE-SEM images of the synthesized samples prepared with different citrate solution pH values and phosphate sources

the consulted pH range 5.0 to 7.6 when the phosphate source is Na_3PO_4, seen in Fig.1(c). The results of the XRD analysis demonstrate that the phase purity of the final product is greatly dependent on the pH of the citrate solution and the phosphate source.

3.2 Chemical composition from ICP analysis

The molar ratios of Ca/P elements in the final products determined by ICP measurements are shown in Table 2. Although the initial Ca/P feeding molar ratio was 1.67, which corresponds to the stoichiometric Ca/P molar ratio in HA, the Ca/P molar ratios in the final products are different. When Na_3PO_4 is used as the phosphate source, the Ca/P molar ratios in the resultants were lower than the stoichiometric value (ranging 1.53-1.59). This suggests that the obtained products are calcium-deficient HA. In addition, the Ca/P molar ratios of the remaining samples were higher than the stoichiometric values (approximately 2.0 with a fluctuation of 0.3). Two aspects may be considered to explain the results: a portion of the product could be derived from

Table 2 Variation of the Ca/P molar ratio in the as-synthesized samples

Sample	Ca/wt%	P/wt%	Ca/P molar ratio
HA11	30.31	14.56	1.61
HA12	20.50	5.22	3.04
HA13	27.12	9.46	2.22
HA14	26.44	10.11	2.03
HA21	23.20	7.23	2.49
HA22	25.54	10.01	1.98
HA23	27.34	9.93	2.13
HA24	28.07	12.53	1.74
HA31	33.60	16.41	1.59
HA32	35.30	17.57	1.56
HA33	35.03	17.43	1.56
HA34	36.70	18.48	1.54

hybrid phases, such as an amorphous phase or other calcium phosphate compounds, and CO_3^{2-} ions can exchange with PO_4^{3-} due to the possible decomposition of citrate molecules.

3.3 Morphology observation

The FE-SEM images of the final products synthesized with various phosphate sources and citrate solution pH values are presented in Fig.2. For the samples synthesized from NaH_2PO_4, a strong variation of the morphology and size of the particles was observed accompanied by the pH changing of the citrate solution. When the pH of the citrate solution changed from 7.6 to 6.0, the sample consisted of a mixture of plate-like and bundle-like particles and the sizes of the particles grew from 0.5-1 μm to 2-4 μm. When the pH of the citrate solution further decreased from 5.5 to 5.0, the bundle-like particles vanished and the sample consisted of a mixture of plate-like and stripe-like particles. Moreover, the number of plate-like particles gradually increased while these of stripe-like particles deceased as the pH decreases. For the samples synthesized using Na_2HPO_4 as the phosphate source, a strong variation of the morphology and size of the particles was observed when the pH of the citrate solution changed from 7.6 to 5.0. For example, the rod-like nanoparticles obtained at pH 7.6 changed to a mixture of rod-like and plate-like nanoparticles at pH 6.0. Additionally, the mixture of hedgehog-like and plate-like particles with micrometer-scale sizes obtained at the pH of 5.5 changed to a mixture of plate-like particles with micrometer-scale sizes at a pH of 5.0. The products obtained with Na_3PO_4 as the phosphate source at a citrate solution pH ranging from 5.0 to 7.6 consist of uniform rod-like nanoparticles with an average size of 30-100 nm in length and 4-10 nm in diameter, respectively. Notably, the decreasing pH value of the citrate solution from 7.6 to 5.0 has no obvious effects on neither the size nor morphology of final HA nanorods.

The information of pH variation and state changes of the reaction solution in the citrate-assisted hydrothermal processes and corresponding resultant products are summarized in Table 3. Combined with the XRD and SEM results, the synthesis of nano-sized products with a pure HA crystalline phase has two characteristics: the final mixture before hydrothermal treatment is milky white, and the pH values of the mixtures after hydrothermal treatment are above 5.7. This suggests that abundant crystallization nuclei form before the hydrothermal treatment consumes the vast majority of calcium and phosphate ions, which restrains crystal further growth to a large extent. Meanwhile, a mixture with sufficient alkalinity after hydrothermal treatment ensures crystal phase purity. In contrast, the micro-sized products with hybrid crystalline phases or no HA crystalline phase were often synthesized under two common synthesis conditions: the final mixture before hydrothermal treatment was a clear or slightly turbid solution, and the pH values of the mixtures after hydrothermal treatment were less than 5.0. This indicates that very few crystallization nuclei formed in the mixture before hydrothermal treatment, and thus, most of the calcium and phosphate ions were used for further

Table 3 Changes in the pH of the solution or suspension in each experimental step

Sample	pH-I	pH-M	pH-H	Crystal phase	Morphology	Size
HA11	5.0	4.02^{c}	4.25	No HA	Plate	Micro
HA12	5.5	4.59^{c}	4.52	No HA	Plate	Micro
HA13	6.0	5.01^{t}	4.93	No HA	Bundle	Micro
HA14	7.6	5.71^{t}	5.20	Hybrid	Bundle	Micro
HA21	5.0	5.10^{t}	4.83	No HA	Plate	Micro
HA22	5.5	6.08^{t}	5.24	No HA	Hedgehog-like	Micro
HA23	6.0	6.86^{m}	5.52	Hybrid	Rod + plate	Nano
HA24	7.6	6.91^{m}	5.76	Pure HA	Rod	Nano
HA31	5.0	6.73^{m}	5.87	Pure HA	Rod	Nano
HA32	5.5	7.96^{m}	6.17	Pure HA	Rod	Nano
HA33	6.0	9.88^{m}	6.77	Pure HA	Rod	Nano
HA34	7.6	12.08^{m}	8.60	Pure HA	Rod	Nano

Note: the superscripts “c”, “t”, and “m” indicate a clear solution, slightly turbid solution, and milky solution, respectively; pH-C refers to the pH of the citrate solution; pH-M refers to the pH of the solution after mixing; pH-H refers to the pH of the solution after hydrothermal treatment

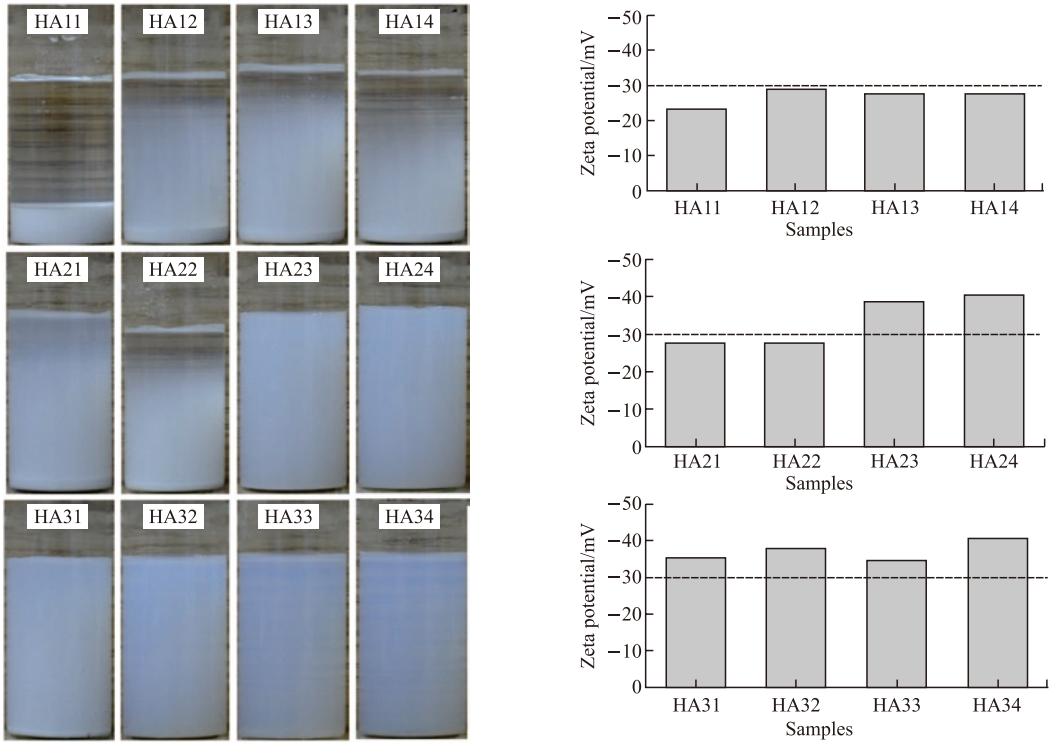

Fig.3 Digital images and zeta potential values of the sample dispersions. The pH value of each dispersion was controlled at 9.5, and the dispersion stood for 24 h before taking each picture

crystal growth. Moreover, a mixture with insufficient alkalinity after hydrothermal treatment ensured crystal phase purity. Notably, micro-sized bundle-like or hedgehog-like products with hybrid crystalline phases were synthesized under two common conditions: the final mixture before hydrothermal treatment was a slightly turbid solution, and the pH values of the mixtures after hydrothermal treatment were between 4.93 and 5.24. This indicates that very few crystal nuclei formed in the mixture before hydrothermal treatment, and most of the calcium and phosphate ions were used for further crystal growth. Moreover, a mixture with insufficient alkalinity after hydrothermal treatment ensured crystal phase purity.

3.4 Colloidal stability evaluation

Additionally, the samples synthesized with different citrate solution pH values and phosphate sources show distinct colloidal stabilities in aqueous dispersions. The authors previously reported that citrate-modified HA nanoparticles could be well dispersed in an aqueous dispersion at pH values ranging from 9 to 10, at which the electrostatic repulsive forces among the particles is strong[7,22,24]. In those regards, different dispersions with particle concentration of 1wt% and pH of 9.5 were prepared and their colloidal stabilities are compared in Fig.3. As shown, HA11-14 and HA21-22 particles are negatively charged with zeta potential absolute values less than 30 mV, and the dispersions of these particles settle significantly after standing for 24 h. These observations can be explained by two aspects: the electrostatic repulsive forces between the particles in the aqueous phase are not strong, and the micro-sized particles have a non-negligible gravity factor. For HA32-34 and HA24, the particles were also negatively charged with zeta potential absolute values above 30 mV. The dispersions of these HA nanorods are almost transparent (slightly milky) and remain homogeneous without any visible sedimentation or creaming over 24 h. The improved colloidal stability is mainly related to the nanometric size of the particles and the sufficient electrostatic repulsive forces between the particles. Although HA23 and HA31 appear colloidal stable and have high zeta potential absolute values (>30 mV), a small amount of sedimentation occurs at the bottom of the sample bottles after standing for 24 h.

Based on the results above, adjusting the pH of the citrate solution and the selection of the phosphate source have significant influences on the synthesis of HA nanoparticles, including the purity of the crystal phase, the size, the morphology, the colloid stability, and the molar ratio of calcium to phosphorus. By optimizing the pH of the citrate solution and the type of phosphate source, uniform rod-like HA nanocrystals with a pure hexagonal crystalline phase, and excellent

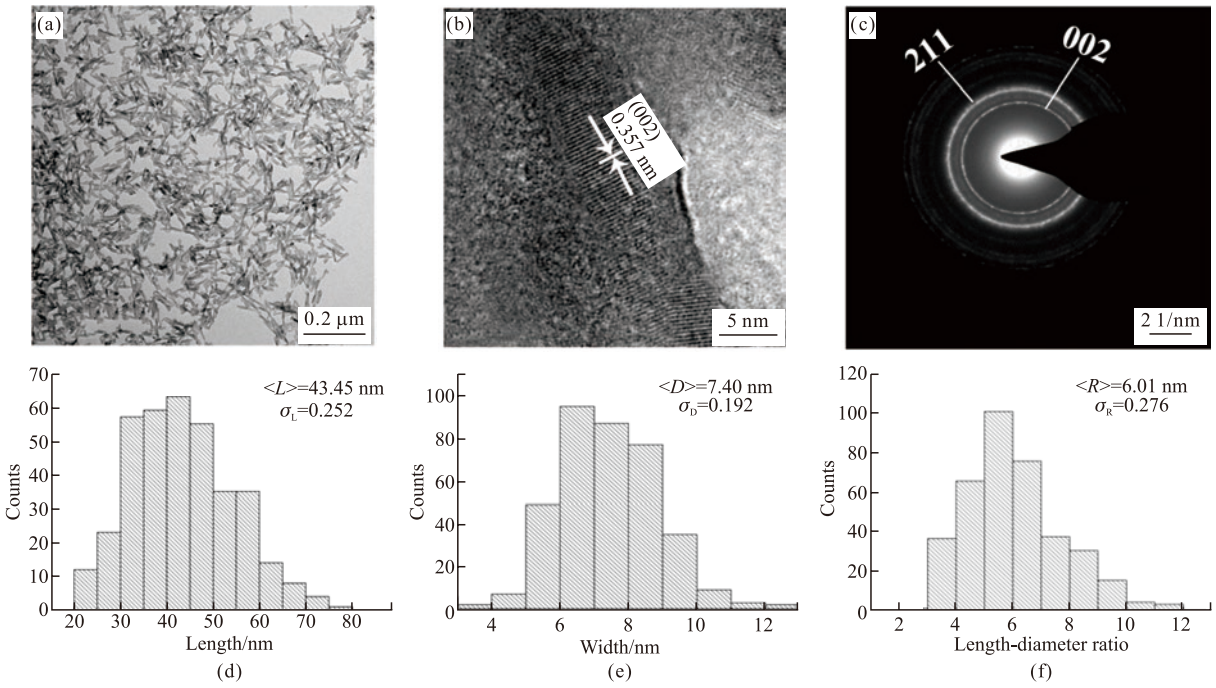

Fig.4 (a) TEM images of the sample HA33 and the static length/diameter ratio; (b) HR-TEM images of the sample HA33; (c) SAED; (d) Specific statistical information on the length; (e) Diameter and (f) Aspect ratio of the particles

colloidal stability in the aqueous phase were successfully synthesized.

3.5 Size statistics of sample HA33

The TEM analysis of sample HA33 is presented in Fig.4. As shown in Fig.4(a), as-prepared HA particles are rod-shaped and uniform in size. No obvious agglomeration between particles was observed, suggesting the strong electrostatic repulsive forces between particles. HRTEM image of the HA nanorods is shown in Fig.4(b). The measured lattice is 0.357 nm, corresponding to the (002) plane of HA. As indicated in the selected area electron diffraction (SAED) pattern (Fig.4(c)), the strong concentric ring patterns can be indexed to the (002) and (211) planes of the hexagonal HA crystallites. Figs.4(d)-4(f) corresponds to the specific statistical information of the length, diameter, and aspect ratio of the particles, respectively. The HA nanorods of sample HA33 exhibit an average length of 43.45 and an average diameter of 7.40 nm, which yields the statistical average aspect ratio of 6.01.

3.6 Liquid crystalline behavior of sample HA33

According to the Onsager theory[33], the driving force for the formation of colloidal liquid crystals in dispersion is in the following: the loss of oriental entropy associated with particle alignment is overcome by the simultaneous gain in excluded volume (configurational) entropy. Generally, an appropriate aspect ratio (length/diameter ratio>4 for rod-like particles), sufficient colloidal stability, and critical particle concentration are three basic criteria that should be met to allow for the formation of a colloidal liquid crystal[34-36]. The characteristics of as-prepared nanoparticles (HA33), including aspect ratio and colloidal stability, meet the requirements for the formation of colloidal liquid crystal.

Permanent birefringence between crossed polarizers depends on the dispersion concentration would serve as the direct evidence for liquid crystalline phase behavior. To verify whether sample HA33 exhibits liquid crystal behavior in its aqueous colloidal dispersion, Fig.5 compares the polarized optical microscopic images of HA33 colloidal dispersions with different particle concentrations. After 1 day, the samples showed stable birefringence when the particle concentration of the dispersion was above 30wt%. No birefringence was observed when the particle concentration of the dispersion was below 27.59wt%. Furthermore, it is worth noting that liquid crystalline behavior of the dispersions changed at various extensions of the settling time. For example, the sample with a 30wt% particle concentration transitioned from a mixture of an isotropic phase and liquid crystalline phase to a completely liquid crystalline phase; the samples with 27.57wt% and 17.7wt% particle concentrations transitioned from a completely isotropic phase to a mixture of an isotropic phase and

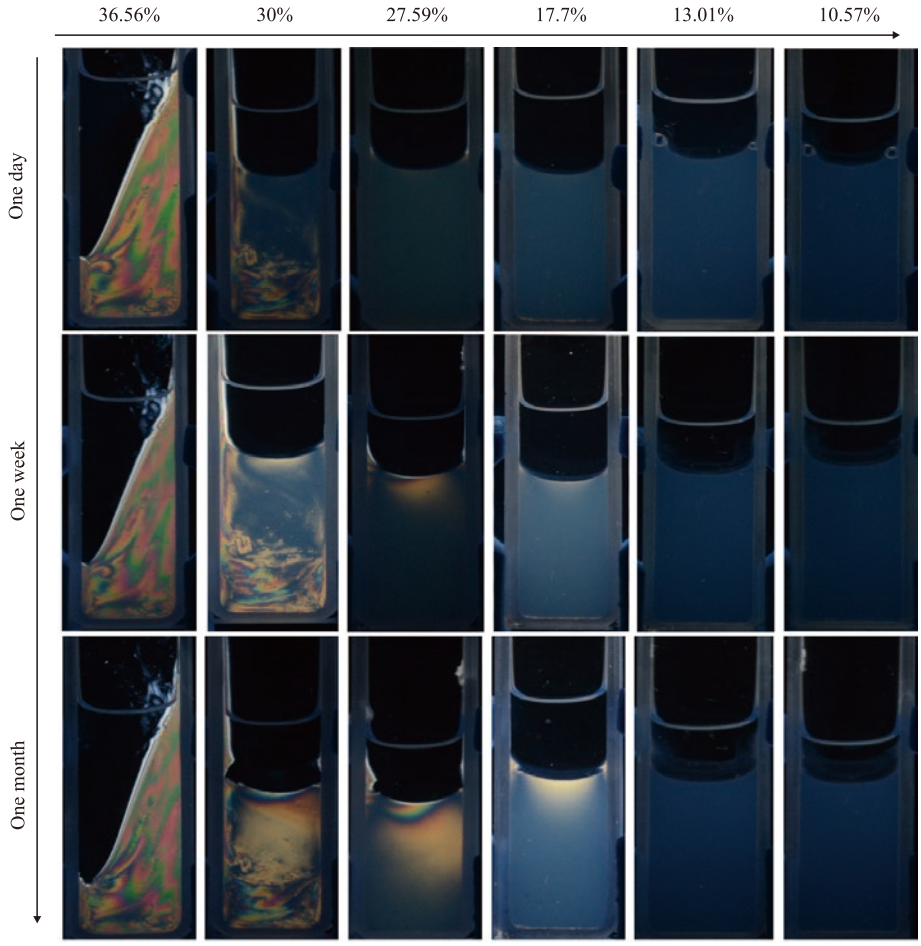

Fig.5 Polarized optical microscopic images of HA33 colloidal dispersions with different concentrations

liquid crystalline phase. These results demonstrate that the pH played a dominant role in the hydrothermal synthesis of the HA nanoparticles. Through the proper optimization of the pH, including the pH of the citrate solution and phosphate solution, well-crystalline HA nanorods with excellent colloidal stability and high aspect ratio were readily achieved. The aqueous dispersion of these HA nanorods underwent a phase transition from an isotropic phase to a liquid crystalline phase, which involves the self-organization of HA nanorods into an ordered structure.

Recently, Nakayama *et al* for the first time observed the behavior of liquid crystals in aqueous colloidal dispersions of polyacrylic-acid-modified HA nanorods[37]. The average length and width of the nanorods were approximately 100 nm and 21 nm, respectively. The aspect ratio of the nanorods was approximately 5.0. The critical concentration for the isotropic state to transition to the liquid crystal state was 7.6vol%, and the concentration of the completely liquid crystal state was above 8.8vol%. Both this study and our current research results show that by controlling the particle morphology, colloidal stability, and dispersion concentration, a liquid crystal state can be achieved in HA colloidal dispersion. This property is very significant for the future design of ordered biomimetic materials and biomaterials.

4 Conclusions

In summary, by controlling the pH of the citrate solution and the type of phosphate source, the phase structure, morphology, and colloidal stability of HA nanorods synthesized with a citrate-assisted hydrothermal method, were significantly changed. The resultant samples exhibited a pure hexagonal phase and excellent colloidal stability and consisted of homogenous rod-like nanoparticles at a citrate solution pH ranging from 5.0 to 7.6 with Na_3PO_4 as the phosphate source. Owing to the excellent colloidal stability and rod-like morphology with a high aspect ratio (>6), the dispersion underwent a phase transition from an isotropic state to a liquid crystalline state as the particle weight concentration increased. The critical concentration of the

phase transition was 17wt%, and the completely liquid crystalline phase was formed at a particle concentration above 30wt%. These novel findings would be helpful for the design of ordered biomimetic materials and biomaterials.

References

[1] Wang L, Nancollas GH. Calcium Orthophosphates: Crystallization and Dissolution[J]. *Chemical Reviews*, 2008, 108(11): 4 628-4 669

[2] Qi C, Lin J, Fu LH, *et al*. Calcium-based Biomaterials for Diagnosis, Treatment, and Theranostics[J]. *Chemical Society Reviews*, 2018, 47(2): 357-403

[3] Hu Y, Gu XY, Yang Y, *et al*. Facile Fabrication of Poly(L-Lactic Acid)-grafted Hydroxyapatite/Poly(lactic-co-glycolic acid) Scaffolds by Pickering High Internal Phase Emulsion Templates[J]. *ACS Applied Materials & Interfaces*, 2014, 6(19): 17 166-17 175

[4] Teotia AK, Raina DB, Singh C, *et al*. Nano-Hydroxyapatite Bone Substitute Functionalized with Bone Active Molecules for Enhanced Cranial Bone Regeneration[J]. *ACS Applied Materials & Interfaces*, 2017, 9(8): 6 816-6 828

[5] Fernando Shanika M, Silva de RM, Silva de KMN. Synthesis, Characterization, and Application of Nano Hydroxyapatite and Nanocomposite of Hydroxyapatite with Granular Activated Carbon for the Removal of Pb^{2+} from Aqueous Solutions[J]. *Applied Surface Science*, 2015, 351(1): 95-103

[6] Googerdchian F, Moheb A. Emadi R, Asgari M. Optimization of Pb(II) Ions Adsorption on Nanohydroxyapatite Adsorbents by Applying Taguchi Method[J]. *Journal of Hazardous Materials*, 2018, 349(5): 186-194

[7] Chen XH, Jin XY, Tan JJ, *et al*. Large-scale Synthesis of Water-soluble Luminescent Hydroxyapatite Nanorods for Security Printing[J]. *Journal of Colloid and Interface Science*, 2016, 468(15): 300-306

[8] Victor SP, Devi MGG, Paul W, *et al*. Europium Doped Calcium Deficient Hydroxyapatite as Theranostic Nanoplatforms: Effect of Structure and Aspect Ratio[J]. *ACS Biomaterials Science & Engineering*, 2017, 3(12): 3 588-3 595

[9] Sun YH, Li YQ, Xu JF, *et al*. Interconnectivity of Macroporous Molecularly Imprinted Polymers Fabricated by Hydroxyapatite-stabilized Pickering High Internal Phase Emulsions-hydrogels for the Selective Recognition of Protein[J]. *Colloids and Surfaces B: Biointerfaces*, 2017, 155(1): 142-149

[10] Li P, Li LL, Zhao YB, *et al*. Selective Binding and Magnetic Separation of Histidine-tagged Proteins using Fe_3O_4/Cu-apatite Nanoparticles[J]. *Journal of Inorganic Biochemistry*, 2016, 156: 49-54

[11] Das P, Jana NR. Length-controlled Synthesis of Calcium Phosphate Nanorod and Nanowire and Application in Intracellular Protein Delivery[J]. *ACS Applied Materials & Interfaces*, 2016, 8(13): 8 710-8 720

[12] Heng CN, Zheng XY, Liu MY, *et al*. Fabrication of Luminescent Hydroxyapatite Nanorods through Surface-initiated RAFT Polymerization: Characterization, Biological Imaging and Drug Delivery Applications[J]. *Applied Surface Science*, 2016, 386(15): 269-275

[13] Zheng X, Liu M, Hui J, *et al*. Ln^{3+}-doped Hydroxyapatite Nanocrystals: Controllable Synthesis and Cell Imaging[J]. *Physical Chemistry Chemical Physics*, 2015, 17: 20 301-20 307

[14] Hu YY, Rawal A, Schmidt-Rohr K. Strongly Bound Citrate Stabilizes the Apatite Nanocrystals in Bone[C]. In: *Proceedings of the National Academy of Sciences of the United States of America*, 2010, 107(52): 22 425-22 429

[15] Wu YJ, Tseng YH, Chan JCC. Morphology Control of Fluorapatite Crystallites by Citrate Ions[J]. *Crystal Growth & Design*, 2010, 10(10): 4 240-4 242

[16] Delgado-López JM, Frison R, Cervellino A,*et al.* Crystal Size, Morphology, and Growth Mechanism in Bio-inspired Apatite Nanocrystals[J]. *Advanced Functional Materials*, 2014, 24(8): 1 090-1 099

[17] Delgado-López JM, Bertolotti F, Lyngsø J, *et al*. The Synergic Role of Collagen and Citrate in Stabilizing Amorphous Calcium Phosphate Precursors with Platy Morphology[J]. *Acta Biomaterialia*, 2016, 49: 555-562

[18] Sandhöfer B, Meckel M, Delgado-López JM, *et al*. Synthesis and Preliminary in vivo Evaluation of Well-dispersed Biomimetic Nanocrystalline Apatites Labeled with Positron Emission Tomographic Imaging Agents[J]. *ACS Applied Materials & Interfaces*, 2015, 7(19): 10 623-10 633

[19] Delgado-López JM, Iafisco M, Rodríguez I, *et al*. Crystallization of Bioinspired Citrate-functionalized Nanoapatite with Tailored Carbonate Content[J]. *Acta biomaterialia*, 2012, 8(9): 3 491-3 499

[20] Yang H, Hao Lj, Du C, *et al*. A Systematic Examination of the Morphology of Hydroxyapatite in the Presence of Citrate[J]. *RSC Advances*, 2013, 3(45): 23 184-23 189

[21] Tsuji T, Onuma K, Yamamoto A, *et al*. Direct Transformation from Amorphous to Crystalline Calcium Phosphate Facilitated by Motif-programmed Artificial Proteins[C]. In: *Proceedings of the National Academy of Sciences*, 2008,105(44): 16 866-16 870

[22] Jin XY, Zhuang JZ, Zhang Z, *et al*. Hydrothermal Synthesis of Hydroxyapatite Nanorods in the Presence of Sodium Citrate and Its Aqueous Colloidal Stability Evaluation in Neutral pH[J]. *Journal of Colloid and Interface Science,* 2015, 443(1): 125-130

[23] Santos C, Almeida MM, Costa ME. Morphological Evolution of Hydroxyapatite Particles in the Presence of Different Citrate:Calcium Ratios[J]. *Crystal Growth & Design*, 2015, 15(9): 4 417-4 426

[24] Jin XY, Chen XH, Cheng YT, *et al.* Effects of Hydrothermal Temperature and Time on Hydrothermal Synthesis of Colloidal Hydroxyapatite Nanorods in the Presence of Sodium Citrate[J]. *Journal of Colloid and Interface Science*, 2015, 450(15): 151-158

[25] Yang H, Wang YJ. Morphology Control of Hydroxyapatite Microcrystals: Synergistic Effects of Citrate and CTAB[J]. *Materials Science and Engineering: C*, 2016, 62(1): 160-165

[26] Jiang D, Li D, Xie J, *et al*. Shape-controlled Synthesis of F-substituted Hydroxyapatite Microcrystals in The Presence of Na2EDTA and Citric Acid[J]. *Journal of Colloid and Interface Science*, 2010, 350(1): 30-38

[27] Martínez-Casado FJ, Iafisco M, Delgado-López JM, *et al*. Bioinspired Citrate-apatite Nanocrystals Doped with Divalent Transition Metal Ions[J]. *Crystal Growth & Design*, 2016, 16(1): 145-153

[28] Iannotti V, Adamiano A, Ausanio G, *et al*. Tampieri, Fe-doping-induced Magnetism in Nano-hydroxyapatites[J]. *Inorganic Chemistry*, 2017, 56(8): 4 446-4 458

[29] Yuan XY, Zhu BS, Tong GS, *et al*. Wet-chemical Synthesis of Mg-doped Hydroxyapatite Nanoparticles by Step Reaction and Ion Exchange Processes[J]. *Journal of Materials Chemistry B*, 2013, 1(47): 6 551-6 559

[30] Fujii S, Okada M, Furuzono T. Hydroxyapatite Nanoparticles as Stimulus-responsive Particulate Emulsifiers and Building Block for Porous Materials[J]. *Journal of Colloid and Interface Science*, 2007, 315(1): 287-296

[31] Sadat-Shojai M, Khorasani MT, Dinpanah-Khoshdargi E, *et al*. Synthesis Methods for Nanosized Hydroxyapatite with Diverse Structures[J]. *Acta biomaterialia*, 2013, 9(8): 7 591-7 621

[32] Lin KL, Wu CT, Chang J. Advances in Synthesis of Calcium Phosphate Crystals with Controlled Size and Shape[J]. *Acta Biomaterialia*, 2014, 10(10): 4 071-4 102

[33] Onsager L. The Effects of Shape on the Interaction of Colloidal Particles[J]. *Annals of the New York Academy of Sciences*, 1949, 51(4): 627-659

[34] Gabriel JCP, Davidson P. New Trends in Colloidal Liquid Crystals based on Mineral Moieties[J]. *Advanced Materials*, 2000, 12(1): 9-20

[35] Davidson P, Gabriel JCP. Mineral Liquid Crystals[J]. *Current Opinion in Colloid & Interface Science*, 2005, 9(6): 377-383

[36] Lekkerkerker HNW, Vroege GJ. Liquid Crystal Phase Transitions in Suspensions of Mineral Colloids: New Life from Old Roots[C]. *Philosophical Transactions of the Royal Society A: Mathematical, Physical and Engineering Sciences*, 2013, 371: 20120263-1-20

[37] Nakayama M, Kajiyama S, Kumamoto A, *et al*. Stimuli-responsive Hydroxyapatite Liquid Crystal with Macroscopically Controllable Ordering and Magneto-optical Functions[J]. *Nature Communications*, 2018, 9(1): 568